THE JOURNAL OF PHYSICAL CHEMISTRY A

ARTICLE

pubs.acs.org/JPCA

Fast and Slow Components in the Crystallization of a Model Multicomponent System, $NaKCa(NO_3)$: The Role of Composition Fluctuations

Ping Wen[†] and Peter Harrowell

School of Chemistry, University of Sydney, 2006 NSW, Australia

C. Austen Angell*

Department of Chemistry and Biochemistry, Arizona State University, Tempe, Arizona 85287, United States

Supporting Information

ABSTRACT: We use calorimetrically detected crystal nucleation and growth studies to broaden the discussion of fluctuation-induced nucleation processes to include composition fluctuations in ionic complex-forming systems. We use the model system $Ca(NO_3)_2$−KNO_3 with $NaNO_3$ introduced as a third component, so that crystallization kinetics can be controlled by change of alkali cation at constant mole fraction of $Ca(NO_3)_2$. At fixed $NaNO_3$ content, we find separate and thermodynamically anomalous kinetics for the crystallization of $NaNO_3$ and $Ca(NO_3)_2$,which we attribute to the importance of slow concentration fluctuations in the latter case. The "nose" of the time−temperature−transformation TTT curve for crystallization of the $Ca(NO_3)_2$ occurs at much higher temperatures and longer times than that for $NaNO_3$ and the shape of the curve is different. Above the metastable liquidus surface of $NaNO_3$, supercooled ternary melts can persist for long times. Suppression of the fast $NaNO_3$ crystallization, by replacement of Na^+ by K^+, is a prerequisite for easy vitrification in this system.

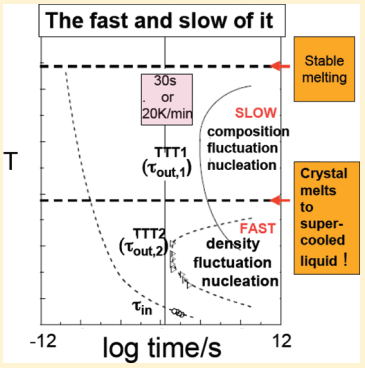

INTRODUCTION

Glasses form when crystals are unable to nucleate and grow to visible proportions during the process of cooling the liquid from its stable state to the final temperature of the experiment, (taken to lie below the glass transition temperature, T_g)[1−4] T_g is commonly defined as the temperature at which the heat capacity of a glass starts to increase abruptly during steady heating at 20 K/min. In most cases it is easily determined by differential scanning calorimetry or differential thermal analysis.[5,6]

It is a common observation that liquids that vitrify on cooling will crystallize when they are reheated at the same rate as they were cooled, though it is often not properly understood why.[7] "Good" glassformers are those that do not crystallize either on cooling to T_g or on reheating anywhere above it. "Ideal" glassformers may be defined as those rare cases that are incapable of crystallizing at any temperature because they are thermodynamically stable as they enter the glassy state. For the latter type of glassformer, an example of which is the eutectic in the system H_2O - $H_2Cr_2O_7.6H_2O$ system,[8] the conventional discussion of glass formation in terms of slowdown of crystal nucleation processes, is irrelevant.[9]

In this paper we deal with the usual case of avoided crystallization and consider the interesting case where the crystallization of the thermodynamically preferred phase exhibits a different and slower kinetics than does that of a less preferred phase of different composition. The thermodynamically preferred phase only appears after the barrier is lowered as a result of the composition change that has occurred, an interesting multicomponent version of the Ostwald "law of stages". To study this question, we use a variant of the much-studied[10−17] system $Ca(NO_3)_2$−KNO_3 in which $NaNO_3$ is included as a third component.[18]

To set up the problem, it will be convenient to discuss the glass formation in terms of relative time scales for the competing processes that determine the outcome of a cooling experiment. For a glass to form, the liquid structure must become arrested (and incapable of further evolution) before a detectable level of crystallization has occurred.[19] The *onset* glass temperature determined in this manner is generally found to correspond to the temperature at which the structural relaxation time (called here the *internal* relaxation time) of the liquid reaches 100 s.[20]

The internal relaxation time of the system is easily determined by dielectric relaxation spectroscopy for molecular liquids. For ionic and metallic glassformers, mechanical or thermal relaxation studies are needed. These various relaxation times are usually

Special Issue: Victoria Buch Memorial

Received: December 13, 2010
Revised: April 18, 2011

 © XXXX American Chemical Society dx.doi.org/10.1021/jp111835z | *J. Phys. Chem. A* XXXX, XXX, 000–000

very similar in magnitude when measured for the same substance,[21−23] though there are some striking exceptions.[21,23,24] The reason that the internal relaxation time becomes long (often with spectacular temperature dependence) is an issue quite separate from the suppression of crystallization and will not be discussed in this paper.

To compare with the internal relaxation time, a characteristic time for crystallization can also be determined by calorimetry.[25,26] In *scanning* calorimetry, a crystallization onset *temperature* is routinely reported, and used in the discussion of supercooled liquid stability, but it has not been linked to a crystallization *time*. A crystallization *time* has been defined from *isothermal* calorimetry studies in which an exothermic peak is observed as crystals nucleate and then grow. The peak corresponds to the maximum crystallization rate but we should note that the completion of the peak only means that the sample is completely crystalline in the case of pure substances. In multicomponent systems, crystallization is terminated by the arrival of the composition at the saturation line (i.e., liquidus line) for the component that is crystallizing, unless the residual (depleted) material becomes too viscous to crystallize. For three dimensionsal (spherical) growth of the crystal, MacFarlane et al.[25b] showed that, under the Avrami nonimpingement assumption, the peak time was reached when the crystallization was 45% complete,

Alternative to the peak of the isothermal crystallization exotherm, the *onset* of the peak may be used, as for the glass transition, to define an *onset* crystallization time. The isotherm for which this time is 100s should be the temperature at which crystallization commenced when temperature is down-scanned at 20 K/s. We will see the test of this proposition in the Results section of this paper. An accord will be dependent on having bypassed the nose of the TTT curve for *nucleation* during the initial cooling in the run for which the crystallization onset temperature is determined.

To understand the latter statement, it is necessary to appreciate that the TTT curve determined by isothermal calorimetry, as normally practiced, is a TTT curve for the combined process, nucleation-plus-growth. The process of nucleation involves smaller length scales than nucleation-plus-growth and is intrinsically faster.[4] The two TTT curves are quite separate in most cases. It is important to recognize this when comparing the results of isothermal crystallization studies with (i) those of computer simulations which see only nucleation, or (ii) results of the classical studies on oxide glassformers, in which the studies were executed by carrying out a nucleation step, and then growing the nuclei to visible proportions for counting. The growth step was conducted at a higher temperature where new nuclei would not form at an interfering rate, implying that the TTT curves obtained were also for nucleation alone. Theoretical studies, both classical[26,27] and more modern density functional approaches,[4] have also been concerned primarily with the nucleation process.[28]

For simple cases where only one crystal is involved (usually single component systems), the form of the TTT curve for nucleation alone can be determined calorimetrically by a different ("two-step") isothermal crystallization protocol,[17,29] but we will not be concerned with this separation in the present paper. Rather, we will be concerned with a different separation, namely, the separation in crystallization kinetics (TTT curves) that is encountered in a multicomponent system where more than one type of crystal forms during the crystallization process. We observe an aspect of liquid crystallization kinetics that is not often discussed at a fundamental level because it is not manifested in the single component systems on which most theoretical studies have been made. It is the effect on the diffusion-controlled part of the TTT curve of the longer range diffusion (or more complex composition fluctuation) that is needed to allow a complex-forming cation like the doubly charged Ca^{2+} species of our mixed nitrate system, to extricate itself from a weak field cation second coordination shell so as to generate a pure crystal of the doubly charged cation.

In the variant of the classical $Ca(NO_3)_2-KNO_3$ system that we use to study these effects (called "CKN" when Ca/K = 4:6), $NaNO_3$ is substituted for KNO_3 to make a "poor" glassformer, and then crystallization resistance is "tuned in" systematically at constant alkali content by substituting K^+ for Na^+. This substitution allows Ca^{2+} to tighten its nitrate anion coordination shell, inhibiting the nucleation of pure $Ca(NO_3)_2$.

This constant 60% alkali nitrate join has the special advantage that the glass temperature, T_g, at which the internal relaxation time reaches 100 s for a standard 20 K/min scan, is almost independent of the composition studied, while the liquidus temperatures and downscan crystallization temperatures change rapidly with composition. The phase diagram for the system is shown in Figure 1.

Because our findings will require understanding of metastable liquidus surfaces, we provide a detailed presentation of the phase relations in the ternary system. Figure 1a shows a 3D representation of how the liquidus surfaces vary with temperature, while Figure 1b shows the quantitative relationships in a 2D contour diagram from the work of Bergmann et al.[18] Thick lines mark the compositions studied in this work.

The use of constant equivalent compositions, requiring that the alkali nitrate corners be represented by $(KNO_3)_2$ and $(NaNO_3)_2$, can be a source of confusion. The model glassformer "CKN" that has been the subject of so many glass science studies, has the molar composition $4Ca(NO_3)_2 \cdot 6KNO_3$, which falls at 43% $(KNO_3)_2$ on the Figure 1b diagram. Because so much of the present study is concerned with compositions that lie on the isocom connecting this composition to one in which $NaNO_3$ replaces KNO_3, we have marked this line conspicuously in Figure 1b. Then we can use the temperature contours of this diagram to understand where the different compositions we study first become supercooled with respect to $Ca(NO_3)_2$. Likewise, we can use constant temperature contours on the $NaNO_3$ liquidus surface to find, by extrapolation, where liquids of the 43% $(MNO_3)_2$ (60% MNO_3) isocom become supercooled with respect to the $NaNO_3$ (the heavy dashed line shows the case of the 170 K isotherm to be encountered later in the paper). Most of the composition variations of this study will involve the variable, x, the fraction of sodium ions in the composition $40CaNO_3)_2 \cdot 60NaNO_3$ that have been replaced by potassium ions, hence defined by x = moles KNO_3/(moles KNO_3 + moles $NaNO_3$).

EXPERIMENTAL SECTION

The materials used in this work were formed directly by the melting of mixtures of reagent grade $NaNO_3$, KNO_3, and $Ca(NO_3)_2 \cdot 4H_2O$ obtained from Sigma-Aldrich, which were used without further purification. The mass of the mixture was about 5 g. Water in the mixture was removed by holding at 573 K for over 12 h in an oven. Then the mixture was heated to a complete liquid state, and quenched into a solid plate of 1.0 mm thickness using a copper mold. Samples of about 15 mg were

dx.doi.org/10.1021/jp111835z |J. Phys. Chem. A XXXX, XXX, 000–000

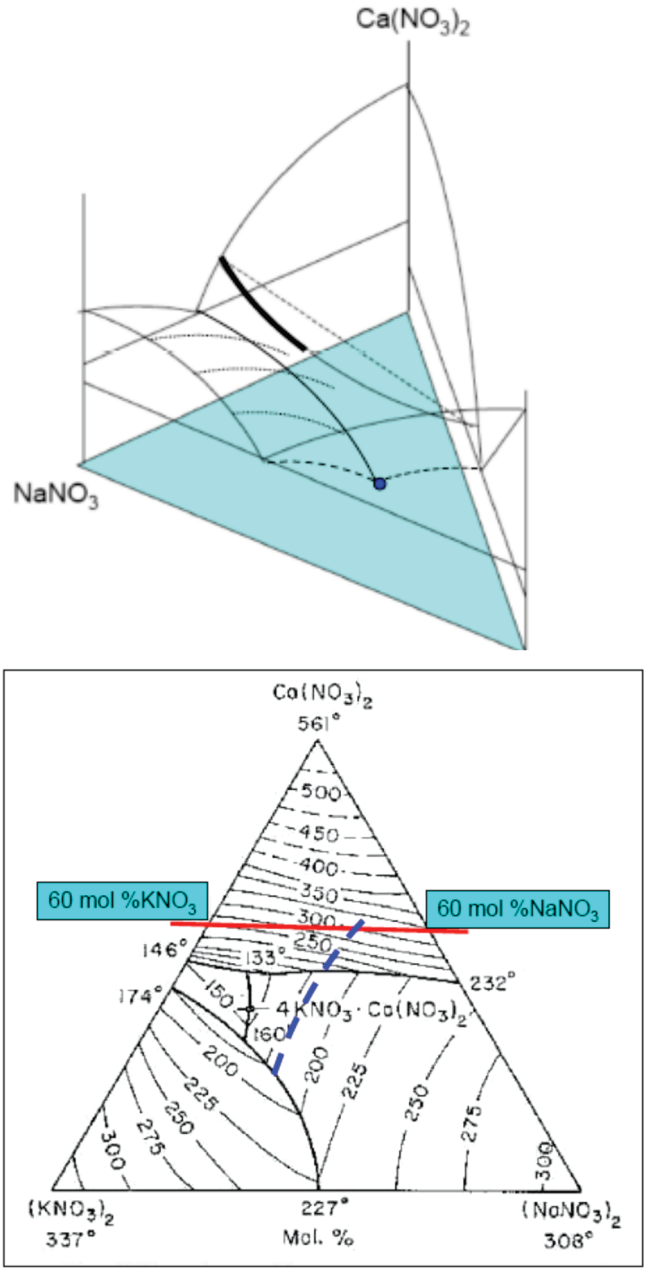

Figure 1. (a) Schematic of the ternary system $NaNO_3$−KNO_3−$Ca(NO_3)_2$ showing liquidus surfaces. The thick solid line represents the liquidus temperatures for compositions explored in this study. Heavy dot is the ternary eutectic. (b) Projection of the liquidus surfaces on to the triangular basal plane, with contour lines for the temperatures in °C (after Bergmann et al.[18]). So that the total electrostatic charge is the same at any point of the diagram, the alkali metal nitrate corners are represented as $(NaNO_3)_2$ and $(KNO_3)_2$. The ternary eutectic lies 13 K below the CKN binary eutectic. The thick dashed line shows a metastable extrapolation of the $NaNO_3$ crystallization surface needed for later discussion. Because the $(MNO_3)_2$ representation confuses many, the position of the 60 mol % $NaNO_3$ to 60 mol % KNO_3 composition isocom, that is the focus of the present study, is marked conspicuously.

broken from the plate and sealed into aluminum DSC pans after further heating to 570 K to minimize water in the samples.

Thermal analysis of phase changes occurring during both cooling and heating schedules was performed using a Mettler Toledo DSC823e thermal analyzer. To obtain completely glassy samples at any composition, the sealed pans were dropped into liquid N_2 from above the liquidus temperatures of Figure 1. Otherwise, the DSC protocols involved cooling from the liquid state at fixed cooling rates, followed by upscans which were conducted in all cases at 20 K/min. According to ref [30], quenching samples in calorimeter pans by dropping into liquid nitrogen produces a cooling rate of 120 K/s or 360 times as fast as our standard 20 K/min heating rate.

XRD studies, that were used to determine the products of initial and secondary crystallization during selected the heating or cooling schedules, will be described in a separate publication focused on the binary $NaNO_3$−$Ca(NO_3)_2$ system.[31]

RESULTS

The present study makes use of results from an initial study of the $NaNO_3$−$Ca(NO_3)_2$ binary system), which is being published separately.[31] A phase diagram containing data pertinent to the present study will appear later in this section. Cooling curves and reheating glass transition and crystallization curves are similar to those seen below for ternary melts and it will help in understanding the rather complex relationships of the present work if two key results of the binary system study are revisited here at the start.

First, and remarkably, $NaNO_3$ was found to crystallize without any supercooling, that is, immediately on crossing the equilibrium liquidus line on the phase diagram (seen in Figure 1b) to lie above 50 mol % $(NaNO_3)_2$. Furthermore, $NaNO_3$ continued to be the primary crystallizing phase well into the $Ca(NO_3)_2$ crystallization field of the phase diagram, including the composition marked 60 mol % $NaNO_3$ in Figure 1b. The reason for this facile crystallization is not well understood, but it is a dominant feature of the present study also. Second, and unremarkably, when $Ca(NO_3)_2$ finally became the primary crystal phase, it appeared with considerable and erratic degrees of supercooling.

Accordingly, the sharp exotherms seen in Figure 2 for heat flow from the samples of different K/Na content, measured during *cooling* from the stable liquid, with exception of $x = 0$ and probably 0.1, are due to $NaNO_3$ crystallization even though this is not expected from the phase diagram. Then, at fixed mole fraction MNO_3 but increasing $K^+/[K^+ + Na^+]$, the exotherms of Figure 2 are due to $NaNO_3$ crystallization though the rate is clearly slowing down as the Na^+ is replaced.

In the binary system, there are circumstances near the eutectic composition where the nucleation rates for $Ca(NO_3)_2$ and $NaNO_3$ are comparable. But as $NaNO_3$ is replaced by KNO_3, $Ca(NO_3)_2$ nucleation is suppressed, showing that the $Ca(NO_3)_2$ crystallization is conditioned by the second nearest neighbor environment. It is suppressed as the Ca^{2+} ions become more firmly locked into their anion environments because K^+ in the second nearest neighbor position is electrostatically less competitive than Na^+.

With increasing $x(KNO_3)$, the nucleation rate for the $NaNO_3$ also decreases. For the cooling rate of Figure 2, 20 K/min, the occurrence of crystallization could be observed at $x = 0.30$ but not beyond. However, as is common, crystallization could be observed in these latter "non-crystallizing" compositions during *reheating*.

To study the recrystallization during reheating over the whole composition range, samples were initially quenched by dropping the sealed pans into liquid nitrogen (LN_2) from above the liquidus temperatures, $T > T_l$. At the 60 mol % alkali nitrate

dx.doi.org/10.1021/jp111835z |J. Phys. Chem. A XXXX, XXX, 000–000

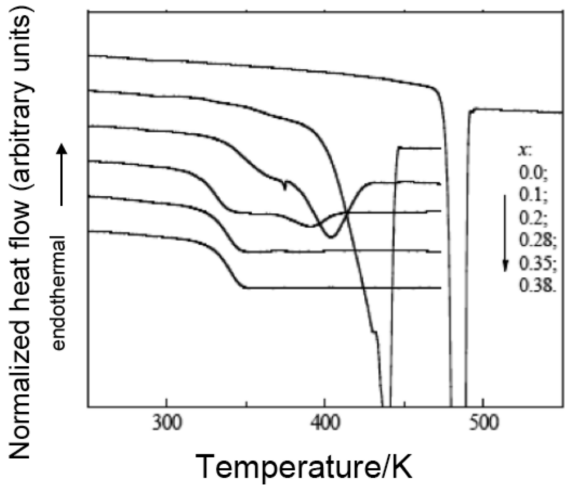

Figure 2. Crystallization exotherms, during cooling at 20 K/min, for the binary $60NaNO_3 \cdot 40Ca(NO_3)_2$ solution and various NaKCa ternary solutions along the $60MNO_3$ join (isocom) seen in Figure 1. x is the fraction $KNO_3/[KNO_3 + NaNO_3]$ in the MNO_3 component of the ternary mixture. The amount of supercooling is shown in a later figure. Note that no crystallization is observed when Na^+ is more than 30% replaced by K^+. These crystallizations, which correspond to $Ca(NO_3)_2$ primary crystals for 20 K/min cooling rates (see Figure 1b) were somewhat irreproducible. The T_c tended to decrease with repetition, perhaps due to removal of heterogeneous nuclei.

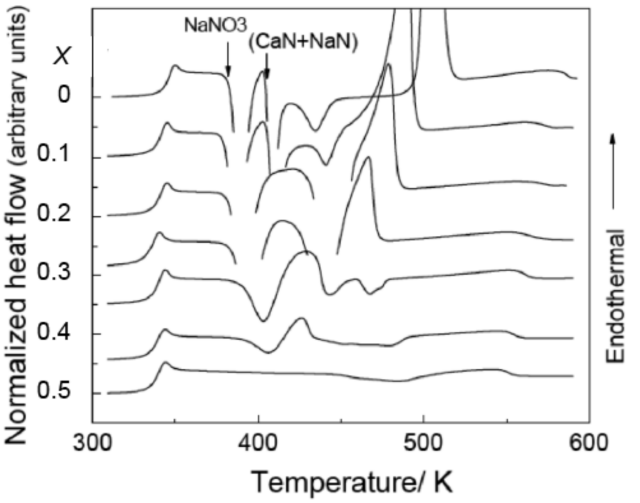

Figure 3. Crystallization exotherms, and subsequent melting endotherms along the 60% MNO_3 isocom, during heating at 20 K/min after quenching to the glass in liquid nitrogen. Again the top scan ($x = 0$) belongs to the binary $(60NaNO_3 \cdot 40Ca(NO_3)_2$. Its slightly higher onset T_g value might be influenced by incomplete suppression of $NaNO_3$ crystallization during the initial quench.

composition of this study, the LN_2 quench suppresses crystallization completely except perhaps in the binary ($Na_{60}Ca_{40}$) case. Results are shown in Figure 3.

Figure 3 shows the recrystallization steps that occur during reheating at 20 K/min after the initial vitrifying quench. Independent of composition, up to about $x = 0.4$, the crystallization occurs sharply at about the same temperature i.e. at the same temperature interval above T_g, implying viscosity control. According to X-ray data, the initial crystallization is exclusively $NaNO_3$ although it is not the most stable product. The crystallization surfaces of Figure 1 are shown extrapolated metastably beyond the ternary eutectic line to illustrate how this prior crystallization of the less stable phase can be possible.

The crystallization of $NaNO_3$, which seems to be complete after some mere 10 K, is followed quickly by a second sharp crystallization peak so long as $x(KNO_3)$ remains small. XRD shows the second exotherm to be due to $Ca(NO_3)_2$ crystal formation, presumably with more $NaNO_3$ in a pseudoeutectic process. With both crystalline phases present, further heating causes a sharp melting which, at $x = 0$ and under equilibrium conditions, would occur at the binary eutectic temperature of 506 K, according to Figure 1b. Because of the fast scan and the excess $NaNO_3$ from metastable crystallization we observe this melting at a somewhat lower temperature, 498 K. The remelting temperature decreases with increasing x, following the pseudoeutectic temperature in the ternary system, see Figure 1.

The slower crystallization of $Ca(NO_3)_2$ at larger mole fractions of KNO_3 is obvious in Figure 3 from the behavior of the second exotherm as the initially sharp peak broadens and becomes shallower before finally disappearing completely at $x = 0.45$. It becomes very sensitive to upscan rate and is finally suppressed completely. As this happens, an interesting effect develops in the lower temperature part of the upscan, which will be seen more clearly in the next figure. It is that, at $x = 0.35$, where the $Ca(NO_3)_2$ crystallization has almost disappeared, the first exotherm (due to $NaNO_3$ crystallization) turns into an endotherm as temperature increases, as if the $NaNO_3$ is remelting. Indeed, in the absence of $Ca(NO_3)_2$ crystals for eutectic comelting this is exactly what the phase diagram predicts will happen. The $NaNO_3$ liquidus projects under the equilibrium $Ca(NO_3)_2$ crystallization surface, and remelting of the $NaNO_3$ will occur as the temperature rises above this liquidus. Figure 1b shows the projection of the 170 °C (443 K) $NaNO_3$ crystallization contour into the metastable composition domain and shows that it intersects our 60% MNO_3 composition line at about $x = 0.35$. This will be remarked on further after the unambiguous results for the composition $x = 0.35$, seen in Figure 4, have been presented.

The decreasing gap between the equilibrium liquidus temperature (of Figure 1b) and T_g (of Figure 3), as KNO_3 replaces $NaNO_3$ along our 60% MNO_3 isocom, is important to understanding the development of good glassformer properties in this system. These trends are summarized in Figure 5, where it is seen that the intersection (at $x \approx 0.4$) of the cooling crystallization line (T_x^c) and heating crystallization temperatures (T_x^h) determines the beginning of the system glassforming range for studies conducted at 20 K/min. We are interested, ultimately, in the possibility of finding third components that give rise to such an intersection even for scans of infinitely slow rate. This would imply that we had engineered an "ideal glassformer". Progress toward such an objective will be described in a separate paper.[32]

Figure 4 shows the consequences of annealing LN_2-quenched samples a little above T_g for different periods (to encourage the rapidly nucleating process) before recooling and conducting the usual 20 K/min upscans. The upscans now show that, unless the annealing has continued for more than 10 minutes, $Ca(NO_3)_2$, the stable phase, is *never* produced (no peak at the $Ca(NO_3)_2$ liquidus at ~300 °C is seen). Rather, the crystallization of the rapidly nucleating phase $NaNO_3$ is completed (at about 130 °C) and then these crystals *remelt*. The melting process finishes at ~160 °C (433 K), according to Figure 4, which is consistent with

dx.doi.org/10.1021/jp111835z |J. Phys. Chem. A XXXX, XXX, 000–000

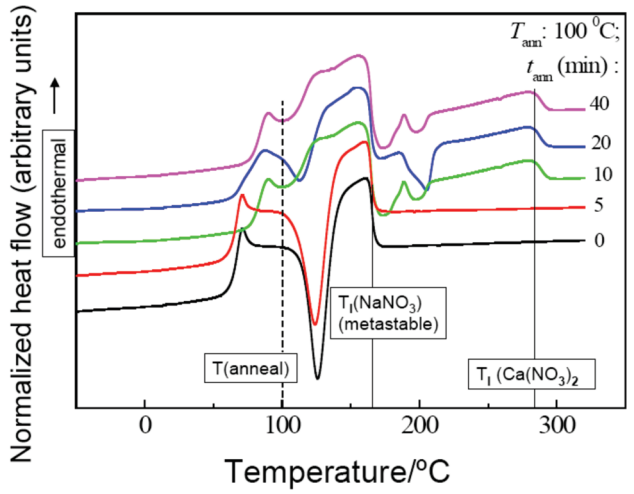

Figure 4. Upscans (in °C for easy reference to Figure 1b) of samples of $x(KNO_3) = 0.35$ initially quenched to the glass in LN_2 and then annealed at 100 °C for different lengths of time before upscanning at 10 K/min. Note the appearance of $Ca(NO_3)_2$ liquidus melting for scans after annealing at 100 °C has been sustained for 10 min or longer. Inspection of the low temperature exotherm shows that after 10 min much of the $NaNO_3$ has crystallized, so that the crystallization of $Ca(NO_3)_2$ has the required composition change. Because no $Ca(NO_3)_2$ ever nucleates for shorter annealing times, this means that in these cases the system is entirely liquid above 170 °C (443 K), the metastable $NaNO_3$ liquidus temperature. At $T = 450$ K, it remains liquid in excess of 8 h, so nucleation of $Ca(NO_3)_2$ takes longer than 3×10^4 s at this temperature and composition. This is indicated by the qualitative addition (solid circle for minimum possible value) for τ_{cryst} for $Ca(NO_3)_2$, marked in later figures (Figures 7 and 9).

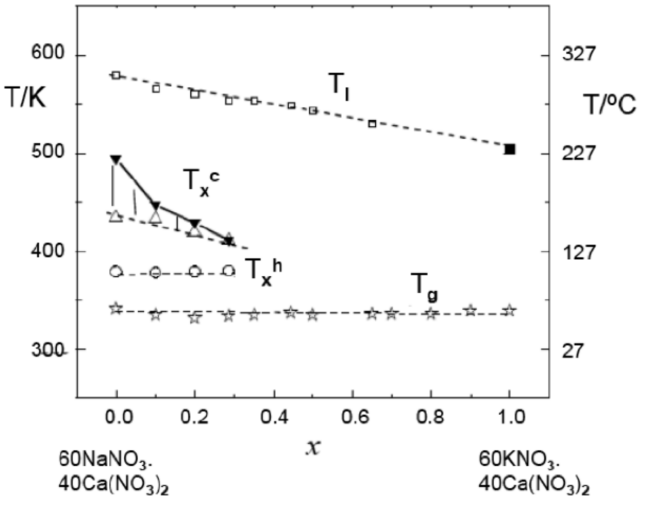

Figure 5. Summary of observations for the isocom $(1 - x)60NaNO_3 \cdot 40Ca(NO_3)_2 - x60KNO_3 \cdot 40Ca(NO_3)_2$: liquidus temperature Tl from Figure 1b: downscan and upscan crystallization temperatures, T_x^c and T_x^h, respectively, obtained from 20 K/min scans and T_g from Figure 3. (filled triangles are from Figure 1 and open triangles are from a later series in which no $Ca(NO_3)_2$ crystallized).

the metastable liquidus temperature of ~170 °C (443 K) obtained by the extrapolation of contours in Figure 1b (thick dashed line) to the composition of our melt. The liquid obtained in this remelting process can be held at 180 °C (453 K) for more

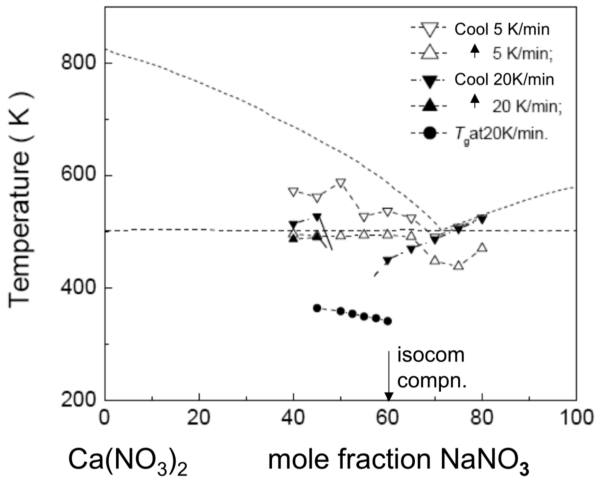

Figure 6. Phase diagram for the binary $Ca(NO_3)_2$—$NaNO_3$ system, showing results of cooling runs at 5 and 20 K/min and glass temperatures for compositions that are fully glassy after LN_2 quenching. Note that, at the isocom composition 60%($NaNO_3$), crystallization of $Ca(NO_3)_2$ was only observed at the slower cooling rate 5 K/min.

than 8 h without any crystals of $Ca(NO_3)_2$ appearing. This important observation is critical to fixing the minimum crystallization time (nose of the TTT curve) for the stable phase relative to the metastable but kinetically crystallizable $NaNO_3$ phase.

$Ca(NO_3)_2$, which nucleated first during 5 K/min cooling at low K^+ contents, is now evidently extremely slow to nucleate despite a supercooling of nearly 150 K, much greater than the (very small, ~25 K) degree of supercooling that provokes the metastable crystallization of $NaNO_3$. Indeed, $Ca(NO_3)_2$ only crystallized if $NaNO_3$ crystallization had occurred first, changing the composition (see Figure 4 caption). Metastables often nucleate first (see ref 28b).

The low temperature nucleation of $NaNO_3$ must be thought of as being driven by supercooling below the projected $NaNO_3$ liquidus temperature of 175 °C (448 K; see extrapolations in Figure 1b), not as driven by supercooling below the much higher $Ca(NO_3)_2$ liquidus temperature.

Holding the liquid at 448 K (where $NaNO_3$ is stable against crystallization) for long enough must, of course, eventually generate the stable $Ca(NO_3)_2$, but it takes more than 3×10^4 s. Escaping the anion coordinated complex structure to nucleate is evidently a very slow process. The minimum crystallization time for $Ca(NO_3)_2$ must occur at temperatures very far above that for $NaNO_3$ and, thus, will seem to be quite disconnected from the glass transition kinetics. Such a disconnection has been seen before for equilibrations in which long diffusion distances are involved, for instance, dyestuff dimerizations in dilute solutions.[33] This is a point of primary importance to the present paper and will be elaborated upon further below.

In Figure 5, we summarize the cooling onset, and heating onset, crystallization temperatures, and show them in relation to the equilibrium liquidus temperatures T_l and the glass transition temperatures T_g. The crystallization product of exotherms observed in downscans at 20 K/min is always $NaNO_3$. The primary crystal *may* be $Ca(NO_3)_2$ but only in the binary system $NaNO_3$—$Ca(NO_3)_2$. When KNO_3 is present, $Ca(NO_3)_2$ crystallization is repressed and, according to X-ray diffraction data, it is then only seen after its concentration has been increased by prior crystallization of $NaNO_3$. If the cooling rate is reduced to

dx.doi.org/10.1021/jp111835z |J. Phys. Chem. A XXXX, XXX, 000–000

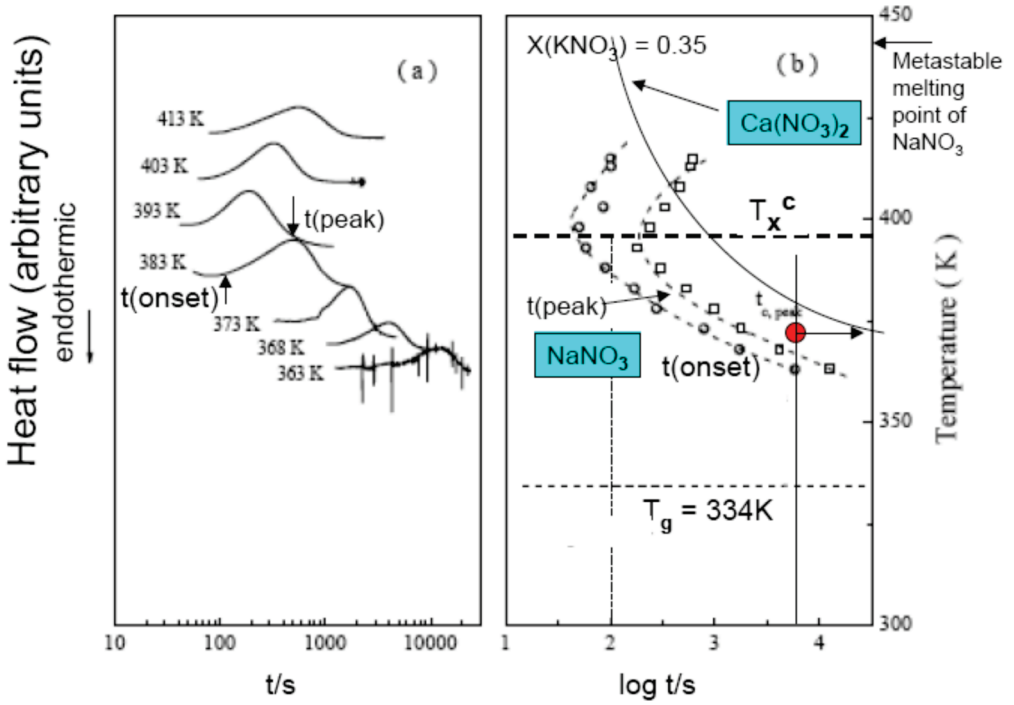

Figure 7. (a) Isothermal crystallization exotherms for the sample $x = 0.35$, held at different temperatures after quenching from above the liquidus. (b) Peak and onset temperatures for the isothermal crystallizations of Figure 7a Filled circle indicates relative location of the *minimum* nucleation time for $Ca(NO_3)_2$ at $T = 370$ K and the solid curve gives the shape that is then implied for the TTT curve for $Ca(NO_3)_2$ lower section. The temperature of onset of crystallization during cooling at 20 K/min is noted for comparison with the isothermal crystallization onset temperature which occurs a little earlier than 100 s.

5 K/min, then in the absence of KNO_3, $Ca(NO_3)_2$ crystallization can be observed, see below.

Because $Ca(NO_3)_2$ primary crystallization in the ternary system is so rare, but is intrinsically so interesting (because of the more complex sort of ion shell fluctuations it requires) we provide, in Figure 6, additional data for the binary system, $NaNO_3 + Ca(NO_3)_2$, in which $Ca(NO_3)_2$ primary crystallization is indeed observed. The liquidus lines in Figure 6 are from ref 10. It is notable how closely these are reproduced by the *cooling* crystallization data, for $NaNO_3$-rich compositions. These are plotted for both 20 and 5 K/min coolings and it is seen that there is essentially *no supercooling* for $NaNO_3$. This contrasts with the $Ca(NO_3)_2$ side of the eutectic composition where supercooling is always observed. Indeed, primary crystallization at our isocom composition is *only* observed if the cooling rate is lowered to 5 K/min. As shown in ref 31, $NaNO_3$ crystallization occurs over the composition range 100−60 mol % $NaNO_3$ even though the eutectic composition is at 72% $NaNO_3$. T_g values for the crystal-free glassforming compositions are included in Figure 6.

In Figure 7, we show the results of isothermal crystallization studies like those described in refs 17 and 26. Part (a) shows the crystallization exotherms and part (b) displays the crystallization onset, also crystallization peak times, in relation to observation temperature, using a log scale. Here we can compare the time for the exotherm onset at a given temperature, with the temperature of onset during upscan at 20 K/min from Figure 4 (not expecting a correspondence) and with the onset temperature during cooling at 20 K/min from Figure 5 (where a correspondence might be expected). This is taken up at the beginning of the Discussion section.

In Figure 8 we show data obtained for fictive temperatures of glasses obtained at different downscan rates, using the modified

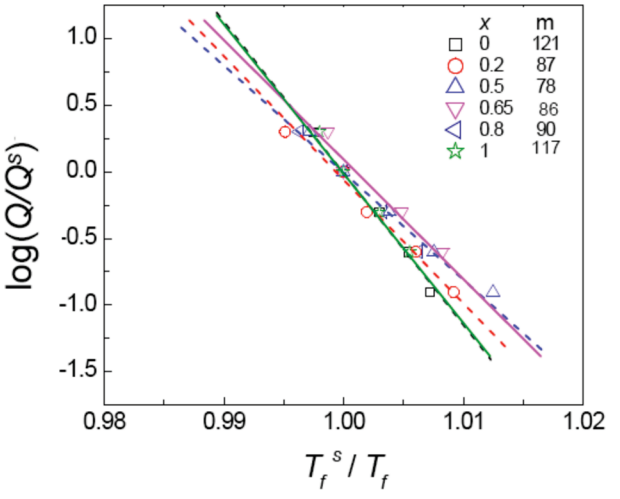

Figure 8. T_f-scaled Arrhenius plot of reduced cooling rates vs inverse fictive temperatures to obtain the m fragilities of compositions along the 40% alkali nitrate tieline in the $NaNO_3^-$ KNO_3−$Ca(NO_3)_2$ system. With $T_f = T_g$, this plot is seen to be an alternate form of T_g-scaled Arrhenius plot of (inverse) relaxation times. An unexpected finding is the systematic variation of the fragility with KNO_3 content, (a sort of "mixed alkali effect" that implies intermediate range ordering of the alkali cations).

Moynihan method of ref 34 for selected compositions across the whole pseudobinary. These are needed for the subsequent construction of Figure 9.

These fictive temperatures, which are temperatures at which structure became frozen during cooling at rate Q K/s, are

dx.doi.org/10.1021/jp111835z |J. Phys. Chem. A XXXX, XXX, 000–000

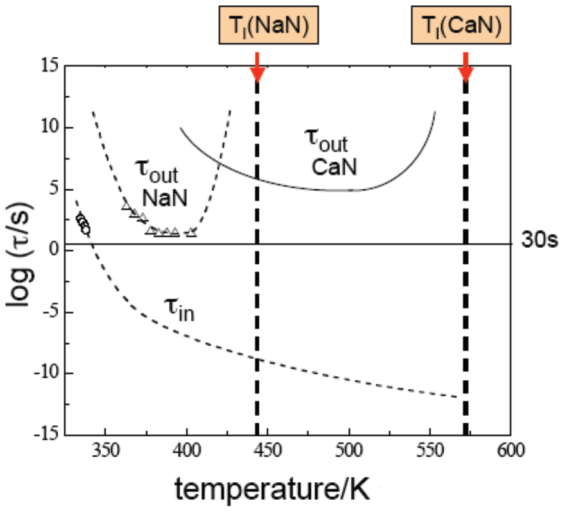

Figure 9. Internal relaxation time (τ_{in}) and isothermal crystallization times (τ_{OUT}) for $NaNO_3$ and $Ca(NO_3)_2$ (qualitative only) at $x(KNO_3)$ = 0.35. The minimum crystallization time for $Ca(NO_3)_2$ cannot be less than 104 s. The slower nucleation of $Ca(NO_3)_2$ must be due to the difficulty of escaping the $Ca(NO_3)_n^{(n-2)}$ complex groups to nucleate (requires slow composition fluctuations).

presented in the reduced form described in ref 34 to allow the direct determination of the fragilities of liquids of different varying alkali mole fractions. The **m** fragility is obtained either from the intercept on the Y axis or from the slope, as explained in ref 34. For the KNO_3 extreme x = 1.0, the very high value, **m** = 117 may be compared with the value reported for this much-studied composition by various previous methods. The value of 117 is significantly higher than the value **m** = 93 reported by Bohmer et al.,[35] but is well supported by the value 125 obtained from a CKN Arrhenius plot included in a survey of viscosities of different substances near their T_g by Tatsumisago, using beam bending viscometry (reported in ref 33).

DISCUSSION

The first point to be discussed is the relation between T_c on heating, T_c on cooling, and the isothermal crystallization time, referring to Figures 2 and 7.

Since the isothermal crystallization protocol we have used does not expose the sample to a fast nucleation zone [20], it should be more closely connected to the cooling crystallization temperature than to that observed on heating up from an initially quenched glass. Thus, we compare the results of cooling samples at 20 K/min (Figure 2) with those of the isothermal crystallization studies (Figure.7). It is notable that the onset of isothermal crystallization occurs after $10^{1.5}$s, that is, 30 s at 410 K and 10 s at the nose, whereas for this composition no crystallization at all was seen in Figure 2 during cooling at 20 K/min. The latter is therefore close to the critical cooling rate[1] for this composition.

It is implied from the above that when the onset of crystallization is observed during cooling, the characteristic onset time for the process is less than 30 s. This time scale is shown as a horizontal line in Figure 9, (the key diagram of this paper, taken up below). This crystallization onset time is a little smaller than, but of the same order as, the 100 s relaxation time attributed to the onset glass transition observed during 20 K/min upscans, and the difference could be attributable to the "dead" time of the experiment needed to reach the temperature of the isotherm of observation. To observe the onset of crystallization during cooling at this composition, then, the cooling rate must be reduced to 10 K/min.

The second point to be emphasized in this discussion is the fact that the crystallization of $Ca(NO_3)_2$ is seen as the *first* crystallization process *only* under conditions of high temperature, slow cooling, and low KNO_3 content, even though it is *always* the thermodynamically stable phase, that is, the one that *should* form first. This points to some important principles controlling crystallization kinetics in complex systems that have not been properly discussed in previous studies. To understand these more fully, we first construct a time/temperature diagram, evolved from Figure 7, in which we compare the internal relaxation time of the liquid (100 s at T_g), with the different crystallization times.

To explain this construction we note that the time scale for formation of any crystal must be infinite right at its thermodynamic liquidus temperature (or melting point in the case of a pure phase) because of the absence of any driving force to crystallize. The time scale then (obviously) decreases as supercooling occurs. The factor that determines whether glasses will form, at a given cooling rate, is the shortest crystallization time that is achieved before crystallization rate reverses at the "nose" of the TTT curve of ref 1 and ref 17. When there are competing crystals, there will need to be more than one TTT curve, one for each of the crystal phases in contention.

To discuss this further we rotate the TTT curve of Figure 7 by 90° (to vertical) to obtain a plot of relaxation time versus temperature, as is normal in consideration of relaxation processes. This gives us Figure 9 in which we can include the *internal* relaxation time, $\boldsymbol{\tau_{in}}$, for the system (as in ref 17 where the shear relaxation time from viscosity was used). Any of the various techniques mentioned in the introduction could be used to establish this internal relaxation time. Here, we use data from Figure 7.

Figure 9 then becomes a relaxation map for the various kinetic processes, nucleation + growth and relaxation, that are possible in this interesting system. We can use it for discussion of the complex interplay of competing crystallizations and meltings that we have documented earlier in the paper. In particular, we emphasize the metastable melting point of the first crystals that form during reheating of the ternary glasses (see Figure 4). This is marked as a vertical thick dashed line at 445 K.

Because Figure 8 shows that the internal relaxation times do not change much with changing KNO_3 replacement of $NaNO_3$ (T_g is nearly invariant in Figure 5), we can see the consequence of the steadily decreasing liquidus temperatures (as $NaNO_3$ is substituted by KNO_3) on the crystallization temperature for the fastest process ($NaNO_3$ crystallization). This must "squeeze" the high temperature part of the TTT curve to lower temperatures, but because its movement is blocked by the constant internal relaxation time, the nose of the TTT curve is squeezed out to longer times, and so the glassforming propensity must increase. The "ideal glassformer" is obtained when the liquidus temperature has been pushed down below the T_g as was observed by Vuillard,[8] for the $H_2Cr_2O_7-H_2O$ eutectic (the likely existence of many such cases is discussed in a current report to *Nature*.)

The limited time range of the calorimetric crystallization measurements seriously restricts what can be said about the long

dx.doi.org/10.1021/jp111835z |J. Phys. Chem. A XXXX, XXX, 000–000

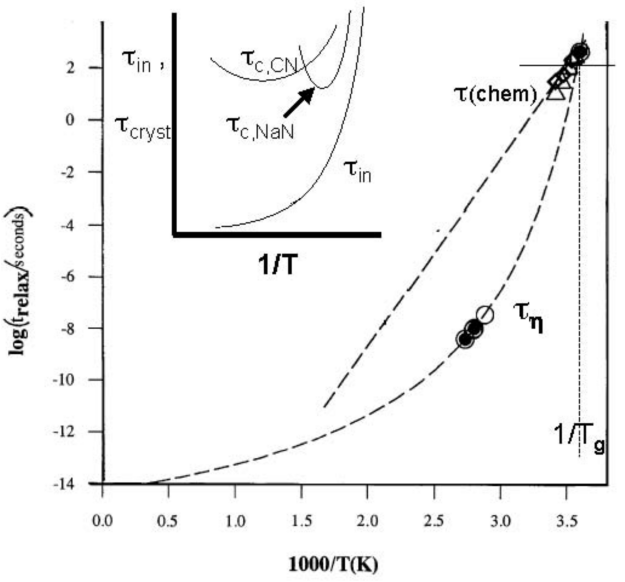

Figure 10. Comparison of simple and complex process time scales and their temperature dependences for two cases: (1) Insert: sodium nitrate vs calcium nitrate crystallization times (τ_c(NaN) vs τ_c(CN) from Figure 9, where they are designated τ_{out}). The low temperature arm of τ_c(NaN) in the insert has a large temperature dependence because it is under the control of viscosity, and therefore images the viscosity relaxation time labeled as τ_{in}. (2) Main figure: chemical order relaxation time vs viscous flow relaxation time for a coordination shell rearrangement in an ionic liquid environment. The different symbols for τ(chem) data points relate to different temperature jumps used in the experiment to check for linear response of the subsequent relaxation process (from ref 37).

time behavior in the present system, but some guidance is available from earlier conductivity-based crystallization studies[36] on LiCl−H_2O solutions that are longer in time scale by 4 orders of magnitude. They were found to smoothly extend the calorimetric determinations,[25] and the depiction of data at longer times in Figure 9 has been based on these older observations. It should also be possible to use the longer time scale conductometric method to determine exactly when $Ca(NO_3)_2$ starts to crystallize in the present system.

An important question is raised by the form of the TTT curve we have had to assign to $Ca(NO_3)_2$ in Figure 9. The question is, why does the crystallization rate of $Ca(NO_3)_2$ below the TTT nose decrease with a *T*-dependence that is initially so different from that of the *internal* relaxation time. Previous studies have shown that the two tend to become parallel as $T \rightarrow T_g$. The answer must lie in the different type of fluctuation needed to produce the $Ca(NO_3)_2$ nucleus. To form the single component $Ca(NO_3)_2$ nucleus, a more complex fluctuation is required, with energy to break up the tightened Ca^{2+} coordination shell and longer distance diffusion for the replacement of K^+ by Ca^{2+} in the second coordination shell .

Such a relationship between temperature dependences for composition-changing fluctuations versus density-changing fluctuations has been seen before. Figure 10 shows the crystallization times for the two branches shown in Figure 9 of the present study as an insert to a figure from an earlier study in which structural relaxation times were compared with chemical order relaxation times. The chemical order relaxation times were deduced from time-dependent optical absorption studies in an ionic melt.[37] They revealed a clear difference between time scales for viscosity on the one hand and for rearrangement of the coordination shell of a transition metal ion (Co^{2+}) on the other. Both the time scales themselves and their temperature dependences are distinct.

The coordination shell rearrangement process is quite similar to the process needed to nucleate a $Ca(NO_3)_2$ crystal in the present multicomponent system. The lower "activation energy" for the process requiring the chemical order fluctuation is common to each case, and is associated with a more physical pre-exponent. Consistent with being a true activated process, and in contrast to the viscous relaxation process, it appears to be an exponential relaxation[37] like other chemical relaxation processes. These have, in common, the feature that their environment relaxes many times during the time necessary for the "target process", that is, the chemical order relaxation or the nucleation process, to occur. Accordingly, such processes would not be expected to exhibit the TTT curves typical of simple glassformers, though their crystal growth rates might still exhibit the "dynamical heterogeneity" signatures common to simple relaxation processes in glass-forming liquids or the crystallization growth rates of single component systems[38] and stoichiometric glassformers.[39]

CONCLUDING REMARKS

The majority of glassforming systems of practical importance are multicomponent in character, and the phenomenology described in this paper must be quite a common occurrence during the crystallization process. To the extent that it is an example of the Ostwald "law of stages",[40] the initial crystallization of a less stable phase should be the most common observation. It is certainly common in posteutectic aqueous solutions, where ice is the fast nucleating phase. Whether or not the detailed crystallization kinetics of the more slowly crystallizing phase follow the pattern we have described here is, however, less certain and must await further investigation. The phenomenon of a crystal phase (here $NaNO_3$) melting to give a supercooled liquid state, is unusual. However it is likely to be shared by aqueous solutions that have precipitated ice during cooling of post-eutectic solutions. Ice is the first crystal to nucleate from solutions in which the extrapolated ice liquidus curve remains above the glass temperature. The idea of ice melting into a metastable state would have been found appealing by Victoria Buch, to whom this work is dedicated.

ASSOCIATED CONTENT

Supporting Information. Additional figures. This material is available free of charge via the Internet at http://pubs.acs.org.

AUTHOR INFORMATION

Present Addresses

[†]Now at the Academy of Sciences, Beijing, China.

ACKNOWLEDGMENT

This work was supported by a grant from the Australian Research Council to Sydney University with Arizona State University in a partner relation.

REFERENCES

(1) Uhlmann, D. R. *J. Non-Cryst. Solids* **1972**, *7*, 337.
(2) Turnbull, D. *Trans. Met. Soc. AIME* **1961**, *221*, 422.
(3) Angell, C. A. *Science* **1995**, *267*, 1924.
(4) Harrowell, P.; Oxtoby, D. W. J. *Chem. Phys.* **1984**, *80*, 1639.
(5) The latter is accomplished with a much simpler apparatus than the former, see ref 6.
(6) Martinez, L. M.; Videa, M.; Mederos, F.; *J. Chem. Educ.* **2007**, *84*, 1222.
(7) Onorato, P. I. K.; Uhlmann, D. R.; Hopper, R. W. *J. Non-Cryst. Solids* **1980**, *41*, 189.
(8) Vuillard, G. *Ann. Chim. (Paris)* **1957**, *2*, 33.
(9) Angell, C. A. *J. Non-Cryst. Solids* **2008**, *354*, 4703.
(10) Protsenko, P. I.; Bergmann, A. G. *J. Gen. Chem. S.S.S.R.* **1950**, *20*, 1367.
(11) Dietzel, A.; Poegel, H. J. *Proceedings III International Congress on Glass*; Garzanti, A., Ed.; Nello Stabilimento Grafico Di Roma Della: Rome, Venezia, 1953; Vol. *1954*, p 219.
(12) Kleppa, O. J.; Hersh, L. S. *Disc. Faraday. Soc.* **1961**, *32*, 99.
(13) Yan, Y.-X.; Cheng, L.-T.; Nelson, K. A. *J. Chem. Phys.* **1988**, *88*, 6477.
(14) Angell, C. A. *J. Phys. Chem.* **1964**, 68.
(15) Mezei, F.; Knaak, W.; Farrago, B. *Phys. Rev. Lett.* **1987**, *58*, 571.
(16) Torell, L. M. *J. Chem. Phys.* **1982**, *76*, 3467.
(17) Senapati, H.; Kadiyala, K. K.; Angell, C. A. *J. Phys. Chem.* **1991**, *95*, 7050.
(18) Bergmann, A. G.; Rassonskaya, I. S.; Schmidt, N. E. *Isvest. Sektora Fis.-Khim Anal., Inst Obshchel Neorg. Khim., Akad Nauk. S.S.S.R.* **1955**, *26*, 156.
(19) Debenedetti, P. G. *Metastable Liquids: Concepts and Principles*; Princeton Univ. Press: Princeton, NJ, 1996.
(20) Angell, C. A. *J. Non.-Cryst. Solids* **1988**, *102*, 205.
(21) Litovitz, T. A.; Sette, D. *J. Chem. Phys.* **1953**, *21*, 17.
(22) Wendt, H.; Richert, R. *J. Phys. Chem.* **1998**, *102*, 5775.
(23) Angell, C. A.; Ngai, K. L.; McKenna, G. B.; McMillan, P. F.; Martin, S. W. *J. Appl. Phys.* **2000**, *88*, 3113.
(24) Wang, L.-M.; Richert, R. *J. Chem. Phys.* **2004**, *121*, 11170.
(25) (a) MacFarlane, D. R.; Kadiyala, K. R.; Angell, C. A. *J. Phys. Chem.* **1983**, *87*, 1094. (b) MacFarlane, D. R.; Kadiyala, K.; Angell, C. A. *J. Chem. Phys.* **1983**, *79*, 3921.
(26) Hillig, W. B.; Turnbull, D. *J. Chem. Phys.* **1956**, *24*, 914.
(27) Yinnon, H.; Uhlmann, D. R. *J. Non-Cryst. Solids* **1983**, *54*, 253.
(28) Zanotto, E. D.; James, P. F. *J. Non-Cryst. Solids* **1985**, *74*, 373. Zanotto, E. D. *J. Non-Cryst. Solids* **1997**, *219*, 42.
(29) Kadiyala, K.; Angell, C. A. *Colloids Surf.* **1984**, *11*, 341.
(30) Wang, L.-M.; Angell, C. A. *J. Non-Cryst. Solids* **2007**, *353*, 3829.
(31) Wen, P.; Harrowell, P. H.; Angell, C. A. manuscript in preparation.
(32) Zhao, Z.-F.; Wen, P.; Harrowell, P. H.; Angell, C. A. manuscript in preparation.
(33) Angell, C. A.; Alba, C.; Arzimanoglou, A.; Böhmer, R.; Fan, J.; Lu, Q.; Senapati, H.; Tatsumisago, M. *Am. Inst. Phys. Conf. Proc.* **1992**, *256*, 3.
(34) Wang, L. M.; Velikov, V.; Angell, C. A. *J. Chem. Phys.* **2002**, *117*, 10184.
(35) Bohmer, R.; Angell, C. A. *Phys. Rev. B* **1992**, *45*, 10091.
(36) Angell, C. A.; MacFarlane, D. R. *Adv. Ceram.* **1981**, *4*, 66.
(37) Martinez, L.-M.; Angell, C. A. *Phys. A* **2002**, *314*, 548.
(38) Ediger, M. D.; Harrowell, P.; Yu, L. *J. Chem. Phys.* **2008**, *128*, 034709.
(39) Nascimento, M. L. F.; Zanotto, E. D. *J. Chem. Phys.* **2010**, *133*, 174701.
(40) Ostwald, W. *Z. Phys. Chem.* **1897**, *22*, 289.